Carbohydrate Polymers 90 (2012) 1725–1731

Contents lists available at SciVerse ScienceDirect

Carbohydrate Polymers

journal homepage: www.elsevier.com/locate/carbpol

Design of deformable chitosan microspheres loaded with superparamagnetic iron oxide nanoparticles for embolotherapy detectable by magnetic resonance imaging

Eun-Young Chung[a], Hyeong-Min Kim[a], Ga-Hyeon Lee[a], Byung-Kook Kwak[b], Ji-Sung Jung[b], Hyo-Jeong Kuh[c], Jaehwi Lee[a,*]

[a] Pharmaceutical Formulation Design Laboratory, College of Pharmacy, Chung-Ang University, Seoul 156-756, South Korea
[b] Department of Radiology, Chung-Ang University Hospital, Seoul, South Korea
[c] Department of Medical Life Sciences, College of Medicine, The Catholic University of Korea, Seoul, South Korea

ARTICLE INFO

Article history:
Received 17 April 2012
Received in revised form 23 July 2012
Accepted 24 July 2012
Available online 31 July 2012

Keywords:
Deformable chitosan microsphere
Superparamagnetic iron oxide
Anti-cancer embolization
Magnetic resonance imaging
Traceability

ABSTRACT

The purpose of this study was to design chitosan microspheres (MS) loaded with superparamagnetic iron oxide nanoparticles (SPIO) suitable for anti-cancer embolotherapy detectable by MRI. Deformable chitosan MS loaded with varying SPIO concentrations (SPIO-chitosan MS) were prepared by ionotropic gelation and a porogenic technique using polyethylene glycol, followed by genipin crosslinking. Adding SPIO nanoparticles to chitosan MS did not significantly affect the chitosan MS morphology. An in vitro phantom study led to selecting SPIO-chitosan MS prepared with 1.0 mM SPIO for an in vivo MR traceability study. SPIO-chitosan MS could be identified following embolization in the renal artery by MRI at 18 weeks. Histological and pathological evidence also showed that SPIO-chitosan MS blocked and remained in the target vessels. Therefore, deformable SPIO-chitosan MS is MR-detectable embolic material with a possible application for anti-cancer embolotherapy.

1. Introduction

Arterial embolization is an anti-cancer therapy that uses embolic materials introduced through a microcatheter to selectively occlude an artery that feeds a tumor, cutting off the vital supply of oxygen and nutrients (Thom, Sigurdson, Bitar, & Daly, 1989). In clinical practice, highly spherical and accurately calibrated microspheres were better for arterial embolization as they could be delivered more distal vessels than irregularly shaped materials, and could more compactly occlude blood vessels (Flandroy et al., 1990). In addition, deformability and softness were essential for easy delivery through the narrow catheter tip (Beaujeux et al., 1996).

Microspheres used for arterial embolization have been made from numerous biomaterials, such as polyvinyl alcohol, trisacryl gelatin, polyhydroxybutyrate (PHB), and polylactide (Bendszus et al., 2000; Grandfils, Flandroy, & Jerome, 1996; Kassab, Piskin, Bilgic, Denkbas, & Xu, 1999; Shomura et al., 2010). Thus, embolic materials currently used in clinical practice are fabricated with synthetic polymers or chemically modified natural polymers. These materials possess their intrinsic safety issues and high cost of synthesis as well as regulatory barriers. However, despite numerous advantages (Agnihotri, Mallikarjuna, & Aminabhavi, 2004; Fischer et al., 2005; Muzzarelli, 2009a, 2010) of chitosan as a biomaterial such as non-toxicity, provision of hemostasis, biocompatibility and biodegradability producing harmless degradation products (amino sugars) it has never been used as embolic materials due to its unsuitable physical characteristics such as brittleness and rigidity (Muzzarelli, 2009b).

Recently, we demonstrated that physical properties of chitosan unsuitable for use as an embolic material could be modified by cross-linking and a porogenic technique. We could produce highly elastic and deformable chitosan microspheres suitable for embolotherapy and exhibited therefore that chitosan is a promising embolic material (Kang et al., 2010).

Embolic microspheres are delivered to the target vessel by a catheter under X-ray angiography guidance. Following the intervention, their location must be monitored to ensure they are occluding the intended blood vessel (Wilson et al., 2003). Thus detectable embolic material would reduce the need for multiple uses of X-ray contrast agents, preventing serious complications and decreasing costs.

Superparamagnetic iron oxides (SPIO) are nanocrystals of iron oxides of magnetite (Fe_3O_4) and/or maghemite (γ-Fe_2O_3), stably coated with hydrophilic polymers, such as dextran, carboxydextran, starch, albumin, silicones, or polyethylene glycol, to prevent

* Corresponding author. Tel.: +82 2 820 5606; fax: +82 2 816 7338.
E-mail address: jaehwi@cau.ac.kr (J. Lee).

0144-8617/$ – see front matter © 2012 Elsevier Ltd. All rights reserved.
http://dx.doi.org/10.1016/j.carbpol.2012.07.058

the particles from aggregating (Thorek, Chen, Czupryna, & Tsourkas, 2006). SPIO is especially popular as a contrast agent for magnetic resonance imaging (MRI) (Moon, 2004). SPIO as an MR contrast agent enormously improves proton relaxation, which is particularly useful for T2-weighted images (Wang, 2011).

By incorporating SPIO nanoparticles into highly spherical and deformable chitosan microspheres, which we previously developed, the microspheres could be detected and visualized by MRI. This property would allow better control of anti-cancer embolization, making the procedure more efficacious and safer (Laurent, 2007). Therefore, the aim of this study was to design and evaluate a novel MR-traceable embolic material for anti-cancer embolotherapy.

2. Materials and methods

2.1. Materials

Chitosan obtained from crab shells (minimally 84% deacetylated, practical grade), poly (ethylene glycol) (PEG) with molecular weight of 20,000 g/mol, iron standard solution for inductively coupled plasma (ICP) spectroscopy (10,000 μg/ml of iron in 4.2%, nitric acid), and lysozyme (from chicken egg white, 70,000 units/mg) were purchased from Sigma–Aldrich Chemical Company (St. Louis, MO). SPIO with hydrodynamic diameter of <80 nm was kindly supplied at 3.33 mg of iron per ml by the Korea Research Institute of Chemical Technology (Daejeon, Korea). Glacial acetic acid, ethyl alcohol, petroleum ether, acetone, and sodium hydroxide were obtained from Duksan Pure Chemical Company (Seoul, Korea). Genipin was purchased from Wako Pure Chemical Industries (Tokyo, Japan).

2.2. Preparation of SPIO-loaded deformable chitosan microspheres (SPIO-chitosan MS)

SPIO-chitosan MS were prepared by ionotropic gelation (Kang et al., 2010). Chitosan (1.5 g) was dissolved in 100 ml of 1% (v/v) acetic acid. PEG (chitosan:PEG = 1:3) was added to 3 ml of the chitosan solution and stirred overnight at room temperature. Then, the SPIO suspension was added to the mixture at various concentrations (0, 0.01, 0.1, 1, 5, and 10 mM) and dispersed homogeneously. The chitosan solution with dispersed SPIO was added drop by drop with the aid of a syringe into coacervation medium using a syringe pump at 0.6 ml/h, and nitrogen gas above the needle (1.0 kgf/cm^2). The upper layer of the coacervation medium was petroleum ether (specific gravity = 0.64 at 20 °C) and the bottom layer was a mixture of ethanol (50 ml) and 10% sodium hydroxide (5 ml). The petroleum ether layer shape the droplets into spheres (Kang et al., 2010), which then solidified in the bottom layer. The solid spheres were dehydrated in acetone and cross-linked with 0.05% genipin for 5 min. The cross-linked microspheres were washed with ethanol then water, three times. Finally, SPIO-chitosan MS were incubated in water for 24 h to extract the PEG, washed with water, and stored in normal saline.

2.3. Visual observation of SPIO-chitosan MS

The SPIO-chitosan MS shape was examined with an optical microscope, fitted with a digital camera (BX60F5, Olympus Optical Co., Ltd., Tokyo, Japan).

2.4. Distribution of SPIO nanoparticles in chitosan microspheres

The SPIO nanoparticles loaded in chitosan microspheres were detected by Prussian blue iron staining (Song et al., 2005). Chitosan microspheres without and with SPIO nanoparticles were fixed in 1% agarose gel. Each 1 cm^3 block was stained with hematoxylin and eosin (H&E) and then Prussian blue. The distribution of SPIO nanoparticles in the chitosan microspheres was examined by light microscopy, as described above.

2.5. Physical characteristics

2.5.1. Diameter and sphericity

The diameter of the microspheres was determined by image analysis software (Optimas 6.1, VSG, UK) attached to the optical microscope. The sphericity was calculated by taking the ratio between the largest and smallest diameters of the microspheres (Table 1).

2.5.2. Loading efficiency

The loading efficiency of SPIO nanoparticles in the microspheres was determined by measuring the iron concentration using an inductively coupled plasma atomic emission spectrometer (ICP-AES; P-5200 ICP system, Hitachi Co. Ltd., Tokyo, Japan) at 259.940 nm. SPIO-chitosan MS (10 mg) were digested in sulfuric acid (95%) and nitric acid (65%) at 70 °C for 3 h to solubilize the iron oxide. After filtering, the solution was diluted with water and assayed by ICP-AES. Concentrations were determined by comparing to a calibration curve of iron (range, 1–50 μg/ml) (Hamoudeh et al., 2007).

2.5.3. Water retention capacity

The water retention capacity of SPIO-chitosan MS was evaluated as an indicator of porosity, which makes the microspheres deformable (Pepper, Reichenberg, & Hale, 1952). After measuring the weight of wet SPIO-chitosan MS (~30 mg), the microspheres were dried at 60 °C for 24 h and the weight was measured again. The degree of water uptake was calculated with the following equation:

$$\text{Water retention}\,(\%) = \frac{W_1 - W_2}{W_2} \times 100$$

where W_1 and W_2 represent the weight of hydrated and dried SPIO-chitosan MS, respectively.

2.6. Release characteristics of SPIO nanoparticles

The release behavior of SPIO nanoparticles from the chitosan microspheres prepared with 1.0 mM of SPIO was examined in two release media for 16 weeks. Twenty milligrams of microspheres was immersed in 30 ml of phosphate buffered saline (pH 7.4) with or without lysozyme at 37 ± 0.5 °C in shaking incubator with shaking at 50 rpm. At predetermined time intervals, samples (0.5 ml) were collected and the iron levels were determined by ICP-AES.

2.7. Scanning electron microscope (SEM) observation

During the release studies, the surface change of chitosan microspheres prepared with 1.0 mM of SPIO nanoparticles in each medium was examined and compared by SEM. The chitosan microspheres were mounted on a metal stub using double-sided adhesive tape, vacuum-coated with platinum using a sputter coater (E-1010 Ion Sputter, Hitachi, Japan), and observed by SEM (Model S-3400N, Hitachi, Japan) at an acceleration voltage of 15.0 kV.

2.8. Microcatheter deliverability

The microcatheter delivery performance of the microspheres was evaluated with the microcatheter (Progreat®, 2.4 Fr, inner diameter 570 μm, Terumo Corp., Tokyo, Japan) used for

Table 1
Physical characteristics of SPIO-chitosan MS.

Samples	Diameter (μm)	Sphericity	Loading efficiency (%)	Water retention (w/w, %)
Blank	545.5 ± 67.5	1.036 ± 0.005	–	35.2 ± 5.6
0.01 mM	541.4 ± 72.8	1.030 ± 0.004	94.7 ± 3.3	32.0 ± 4.2
0.1 mM	545.5 ± 83.2	1.041 ± 0.010	97.3 ± 4.1	30.0 ± 2.8
1.0 mM	543.2 ± 85.6	1.016 ± 0.008	96.6 ± 3.3	28.1 ± 3.3
5.0 mM	535.5 ± 94.5	1.012 ± 0.003	95.5 ± 2.8	25.5 ± 4.1
10.0 mM	545.5 ± 81.1	1.021 ± 0.005	95.5 ± 3.4	22.7 ± 3.3

Table 2
MRI parameters for the MR images of the in vitro phantom study.

Sequence	TR (ms)	TE (m)	FOV (mm)	Thickness (mm)	ETL	FA	Resolution	NEX
T2WI-FFE	643	9.2	250 × 250	1.5	1	30	673 × 673	1
T2WI-TSE	2128.7	80	250 × 250	1.5	15	90	700 × 600	8

T2WI: T2-weighted image, FFE: Fast field echo technique, TSE: Turbo spin echo technique, TR: Repetition time, TE: Echo delay time, FOV: Field of view, ETL: Echo train length, FA: Flip angle, and NEX: Number of excitation.

transcatheter arterial embolization. Fifty milligrams of the SPIO-chitosan MS loaded with 1.0 mM of SPIO was suspended in 1 ml of normal saline and X-ray contrast agent (Visipaque™, GE Healthcare, UK) (50/50, v/v). The suspension was loaded into a 1 ml syringe and manually injected through the catheter. Ease of passage through the microcatheter during injection was measured and changes in the microsphere appearance during the transition through the microcatheter tip were observed by optical microscopy.

2.9. In vitro phantom study of MR traceability of SPIO-chitosan MS

An MR phantom study was carried out to measure MR traceability and to determine the optimal concentration of SPIO nanoparticles for an in vivo study. The chitosan microspheres were loaded with various concentrations of SPIO nanoparticles, ranging from 0 to 10.0 mM. The SPIO-chitosan MS were fixed in 1% agarose gel blocks (1 cm^3) and T2-weighted images were taken under the operational parameters described in Table 2 using a 3.0 T MRI device (Achieva, Philips, Eindhoven, The Netherlands).

2.10. In vivo MR traceability study of SPIO-chitosan MS

White male New Zealand rabbits weighing approximately 2.5 kg were used to evaluate the traceability of SPIO-chitosan MS. Rabbits were anesthetized by intramuscular injection of 0.4 ml zolazepam hydrochloride (17 mg/kg, Virbac, Carros, France) and 0.8 ml xylazine hydrochloride (4 mg/kg, Bayer Korea, Seoul, Korea). In an angiographic suite (Axiom Artis, Siemens Inc., Erlangen, Germany), a 4-F angiography cobra catheter (Terumo, Tokyo, Japan) was inserted through the right femoral artery. SPIO-chitosan MS (~100 mg) prepared with 1.0 mM of SPIO was injected into the right renal artery, under fluoroscopy, until the artery was totally occluded. MRIs of the embolized renal artery were obtained for 18 weeks to confirm the MR-detectability of the microspheres. MRI was performed on a 3.0 T MRI device using a surface coil (SENSE-Knee-8; Philips). MRIs of the rabbit were T2-weighted images obtained by Turbo Spin Echo (TSE) and Fast Field Echo (FFE) techniques. The detailed operational parameters are described in Table 3.

2.11. In vivo embolization study

Two weeks after embolization, the rabbit was euthanized by intravenous injection of 10 ml of 2 M potassium chloride. Both embolized right kidney and unembolized left kidney were cut in half along the sagittal plane for pathologic examination. The hilum of the kidney was sliced along the coronal plane for an occlusion test. The SPIO-chitosan MS occluding the kidney vessel was examined by iron staining with Prussian blue.

3. Results and discussion

3.1. Visual observation of SPIO-chitosan MS

The morphological features of microspheres were visualized by optical microscopy. The chitosan microspheres were spherical with a smooth surface. The SPIO-chitosan MS were dark-brown in color, which originates from the SPIO. Higher SPIO concentrations resulted in a darker surface color (Fig. 1). Based on the paper published by Yuan et al. (2007), chitosan microspheres exhibited bluish color after crosslink with genipin for 4, 8 and 16 h. And an increase in bluish color was obvious with increasing crosslinking time. However, crosslinking time in our study was only 5 min and thus, blue color could not be observed.

The shape and surface morphologies of blank chitosan microspheres did not differ significantly from SPIO-chitosan MS, except for color.

3.2. Distribution of SPIO nanoparticles in chitosan microspheres

Blank chitosan MS and SPIO-chitosan MS were stained with H&E and Prussian blue to examine the distribution of SPIO nanoparticles in chitosan microspheres. SPIO-chitosan MS with higher SPIO concentrations (Fig. 2D and E) exhibited blue in color because of the iron of SPIO nanoparticles stained with Prussian blue (Rice et al., 2007). Blank chitosan microspheres, however, were red (Fig. 2A), and did not stain with Prussian blue. Thus, we were able to determine that SPIO nanoparticles were homogeneously dispersed in the chitosan microspheres.

3.3. Physical characteristics

The mean diameter of the blank chitosan MS and SPIO-chitosan MS was about 540–550 μm, which is appropriate for embolizing the rabbit renal artery. The SPIO nanoparticle concentration did not significantly change the chitosan microsphere size (Table 1). The sphericity of the chitosan microspheres was between 1.012 and 1.041, which was better than or similar to blank chitosan microspheres (1.036). Anticancer embolotherapy has usually been performed in clinical practice when therapeutic surgery cannot be carried out such as severe hepatoma (Llovet et al., 2002). In the anticancer embolotherapy, efficient occlusion of the target blood

Table 3
MRI parameters for the MR images of in vivo study.

Sequence	TR (ms)	TE (ms)	FOV (mm)	Matrix size	Thickness (mm)	NEX
T2WI-FFE	562	9	150 × 150	244 × 320	2.0	8
T2WI-TSE	2222	100	150 × 150	236 × 320	2.0	12

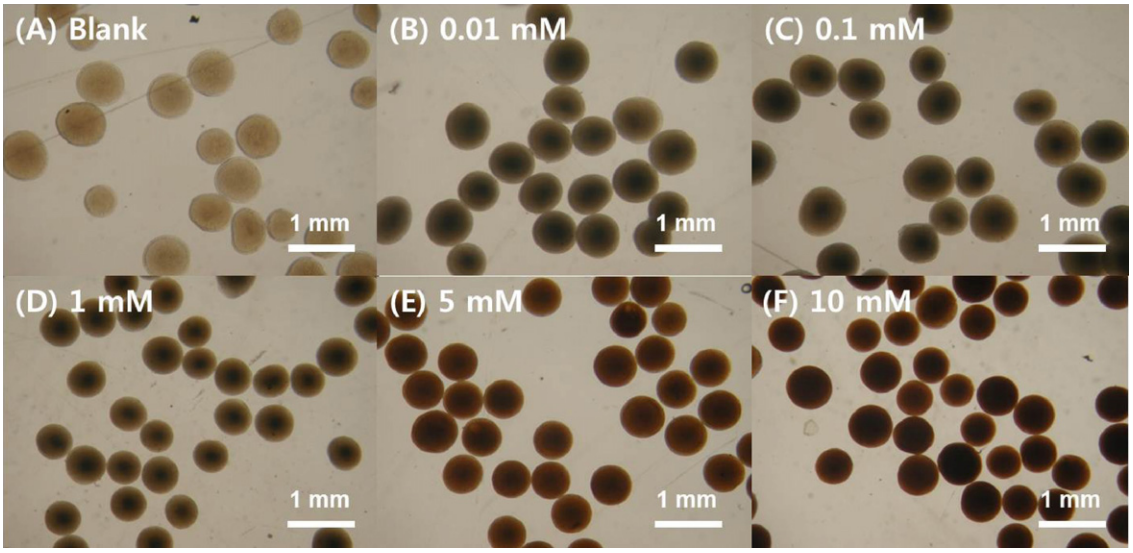

Fig. 1. Morphological features of the chitosan microspheres loaded with various SPIO concentrations. The images show chitosan microspheres prepared without SPIO (A), with 0.01 mM (B), 0.1 mM (C), 1.0 mM (D), 5.0 mM (E) and 10.0 mM of SPIO (F).

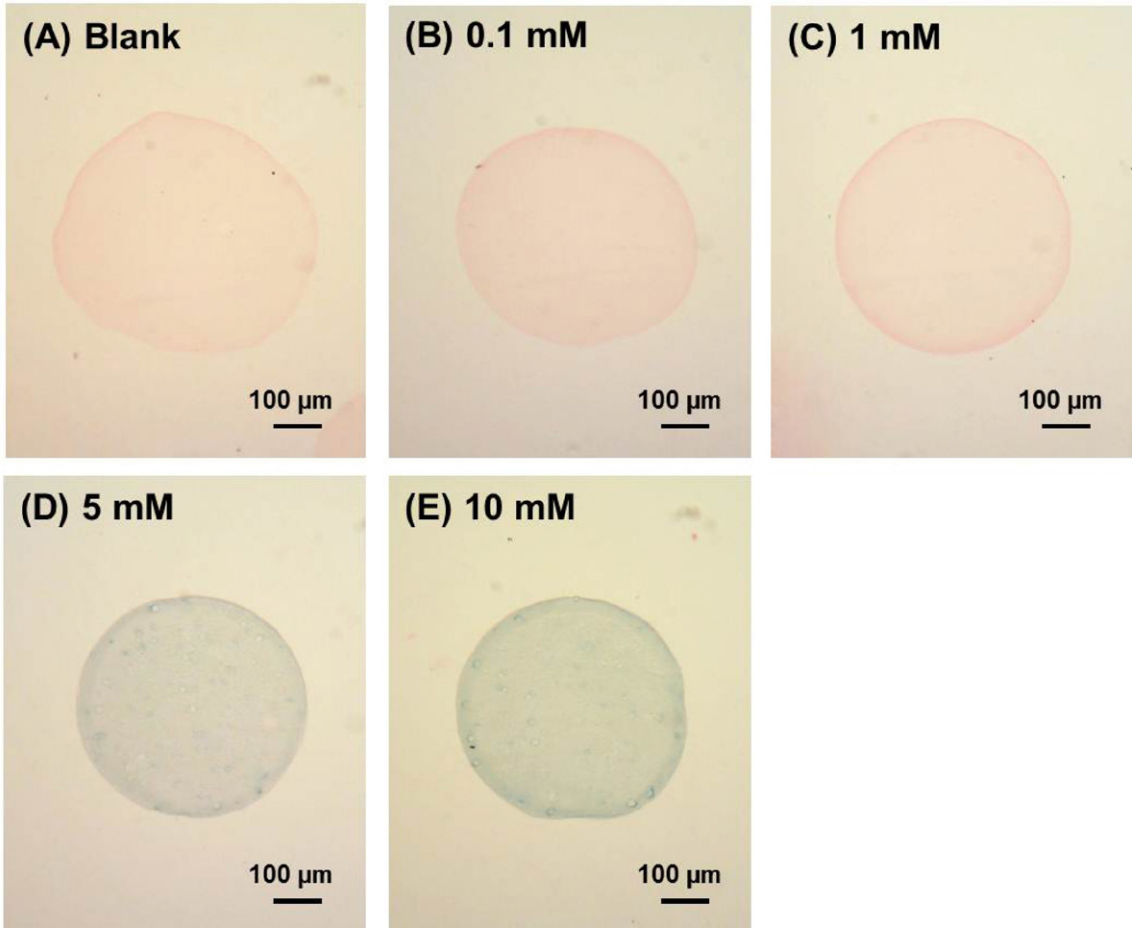

Fig. 2. Optical micrographs of blank chitosan MS and SPIO-chitosan MS stained with H&E and Prussian blue. The blank chitosan MS and SPIO-chitosan MS prepared with 0.1 and 1 mM SPIO were observed to be red in color while SPIO-chitosan MS prepared with 5 and 10 mM SPIO were blue in color because the iron of SPIO was clearly stained by Prussian blue. (For interpretation of the references to color in this figure legend, the reader is referred to the web version of the article.)

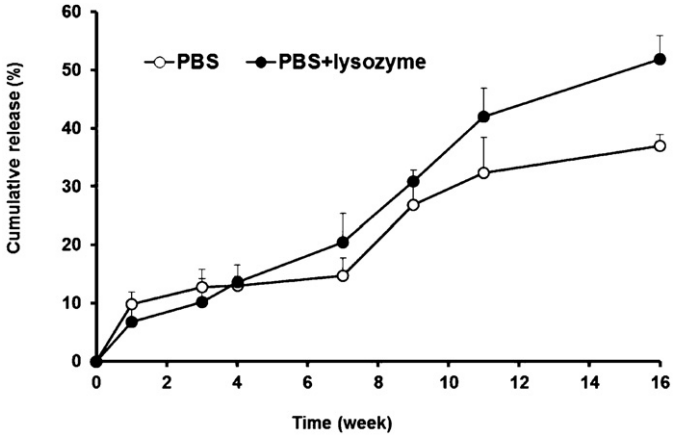

Fig. 3. The accumulated release profiles of SPIO nanoparticles from chitosan microspheres at 37 ± 0.5 °C in PBS (pH 7.4) alone and with lysozyme (mean ± SD, $n = 3$).

vessel feeding tumor tissues is considered to be a key factor and this has been successfully achieved by using highly spherical shape of embolic materials that fit the size of the vessel (Bendszus et al., 2000).

The loading efficiency of SPIO nanoparticles in chitosan microspheres was over 94% for all microspheres (94.7–97.3%). This result clearly implies that there was minimal SPIO nanoparticle loss when producing SPIO-chitosan MS by ionotropic gelation. Moreover, the amount of SPIO nanoparticles loaded in the chitosan microspheres rarely affected physical characteristics (Table 1).

The water retention capacity was measured to determine the porosity of the microspheres, since porous microspheres are more elastic and deformable preferred for chemoembolization (Derdeyn, Graves, Salamat, & Rappe, 1997). The water retention value decreased proportionally with increasing SPIO nanoparticles added (Table 1). This may due to SPIO nanoparticles occupying the void space within the chitosan matrices.

3.4. Release characteristics of SPIO nanoparticles

The in vitro release of SPIO nanoparticles from chitosan microspheres in PBS and PBS with lysozyme (70,000 units/vessel) was compared to examine the impact of lysozyme upon the SPIO release from the microspheres and chitosan degradation. Lysozyme is a muramidase found in most body tissues and blood that depolymerizes chitosan (Hultmark, 1996). Within 16 weeks, about 50% of the initial SPIO nanoparticles were released in PBS with lysozyme, while about 30% of SPIO nanoparticles were released in PBS without lysozyme during the same period (Fig. 3). SPIO nanoparticles were probably released faster in PBS containing lysozyme than PBS without lysozyme because the lysozyme degraded the chitosan matrices. Although more than 20% of SPIO was released in PBS with lysozyme at 16 weeks, SPIO-chitosan MS were traceable by MRI for at least 18 weeks, according to in vivo studies in rabbits.

3.5. SEM observation

SEM was carried out simultaneously with the release test, lasting 16 weeks. When chitosan micromatrices were immersed in PBS or PBS with lysozyme, water permeated into the micromatrices making them swell. However, accompanying the hydration process, bond cleavage and degradation of chitosan were obviously occurred in PBS with lysozyme (Ren, Yi, Wang, & Ma, 2005). By this procedure, therefore, when observed after 6 weeks, more porous structure on the surface was noticeably observed in PBS with lysozyme compared to in PBS alone by SEM. Upon examination of photomicrographs obtained after 10 weeks the porous structure on the surface of the microparticles in PBS with lysozyme became clearer, compared to that in PBS alone. Due to the enhanced degradation property of chitosan embolic microparticles in PBS with lysozyme, the size change of the microparticles in PBS with lysozyme was also greater than that in PBS, especially after 16 weeks, as illustrated in Fig. 4. Other studies have also reported that lysozyme degrades chitosan microparticles (Muzzarelli, 1993; Ren et al., 2005), which would increase the release of SPIO-chitosan MS in lysozyme-based medium.

3.6. Microcatheter deliverability

In clinical practice, SPIO-chitosan MS are delivered to the target vessel with a syringe attached to a microcatheter. In this study, some SPIO-chitosan MS were bigger than the microcatheter tip. SPIO-chitosan MS with sizes of 543.2 ± 85.6 μm in diameter were still delivered through the microcatheter (inner diameter of the tip = 570 μm). As the particles moved through the microcatheter to the distal tip, they deformed slightly. The particles then returned to their original shape without any signs of damage after leaving the catheter tip. The SPIO-chitosan MS were deformable due to the porous structure of the microspheres, formed by leaching the PEG. Thus, the SPIO-chitosan MS was easily delivered through a microcatheter for embolization (Derdeyn et al., 1997).

3.7. In vitro phantom study of MR traceability of SPIO-chitosan MS

Phantom experiment using SPIO-chitosan MS prepared with various SPIO concentrations (0, 0.01, 0.1, 1.0, 5.0 and 10.0 mM) was performed to determine the proper SPIO concentration for in vivo MR traceability. The phantom images showed increasing the SPIO nanoparticle concentration made the microspheres bigger and darker (Fig. 5). The SPIO-chitosan MS with 1.0 mM SPIO generated the most obvious MR image reflecting the actual size of the chitosan microspheres. Therefore, a SPIO concentration of 1.0 mM was considered to be suitable for in vivo studies. The SPIO concentrations less than 1.0 mM resulted in an unrecognizable shape. Concentrations exceeding 1.0 mM showed excessively aggregated and overlapped images, with SPIO-chitosan MS that was hard to distinguish from the background. This result shows that SPIO-chitosan MS with a suitable SPIO concentration can be traced by MRI following embolization therapy.

3.8. In vivo MR traceability study of SPIO-chitosan MS

SPIO-chitosan MS were injected into the right renal artery of rabbits to embolize the kidney. The left kidney was left as a control. We obtained T2-weighted images of the rabbit using TSE and FFE sequences, because SPIO enhances the contrast of T2-weighted MR images (Qiao, Yang, & Gao, 2009). TSE sequence was used because it is the most routine sequence in clinical practice (Escobedo et al., 1996). FFE was used since the SPIO signal is stronger using FFE than TSE (Chung, Yamada, & Yang, 2009, chap. 5: unit 5A.3).

SPIO-chitosan MS was best visualized by T2-weighted images using the FFE sequence. The dark signals from SPIO-chitosan MS were detected around the main renal artery and segmental artery of the embolized kidney for 18 weeks after embolization. The MRI confirmed that SPIO-chitosan MS efficiently blocked the target blood vessels for 18 weeks.

Changes in sizes of both the embolized and unembolized kidneys were detected by MRI. The embolized kidney remained similar in size to the unembolized kidney for 2 weeks. At 8 and 18 weeks after embolization, however, a gradual decrease in the size of embolized kidney became obvious. The embolized kidney

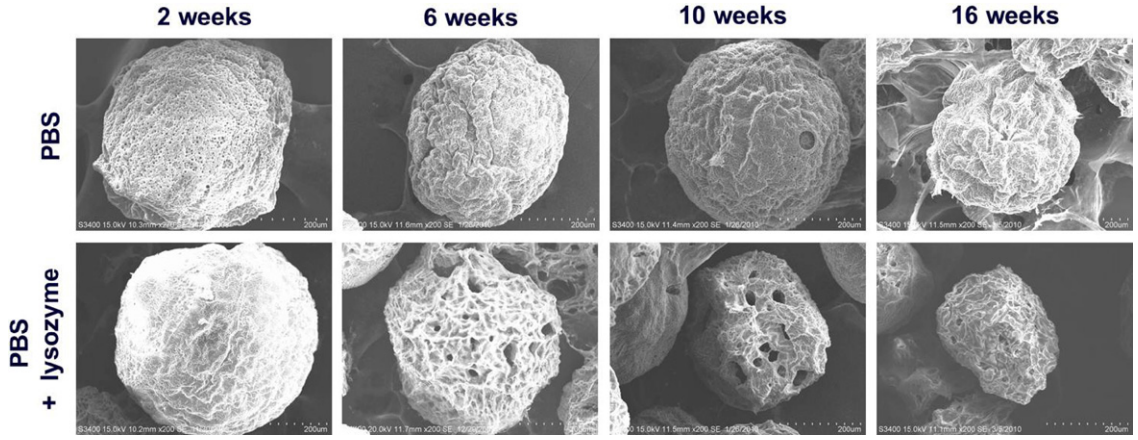

Fig. 4. Scanning electron micrographs of SPIO-chitosan MS prepared with 1.0 mM SPIO in PBS (pH 7.4) alone and with lysozyme for 16 weeks.

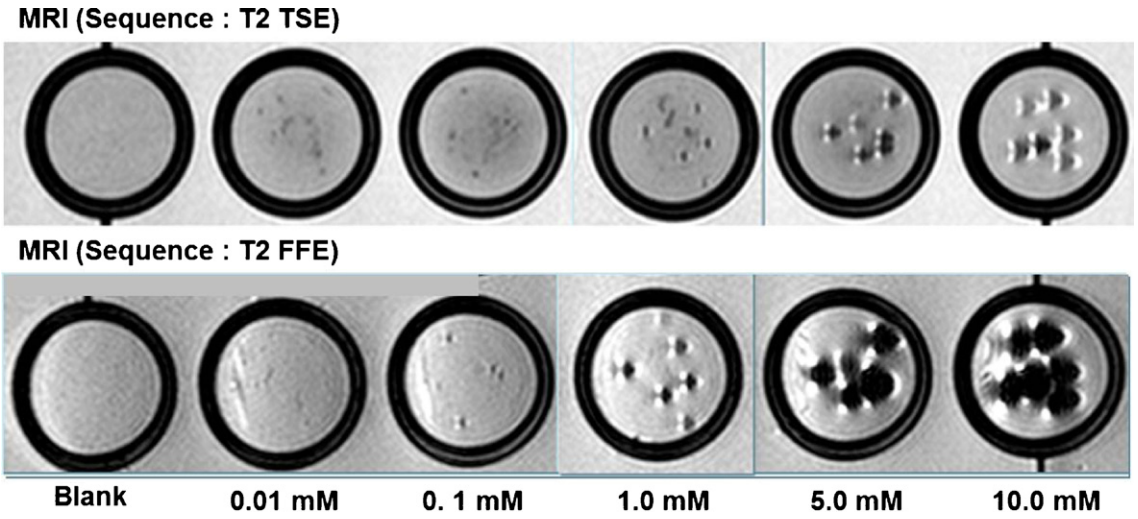

Fig. 5. T2-weighted MR images of an in vitro phantom model of chitosan microspheres loaded with various concentrations of SPIO.

atrophied, due largely to loss of renal function caused by blocking the blood supply. On the other hand, the size of unembolized kidney increased considerably due to compensatory renal hypertrophy following damage of the opposite kidney (Widmaier, Raff, & Strang, 2006).

These results clearly demonstrate that SPIO-chitosan MS prepared with 1.0 mM SPIO could be detected by MRI for 18 weeks after embolizing rabbit kidneys. This property of SPIO-chitosan MS allows MRI assessments of continued occlusion of the target blood vessel after embolotherapy.

3.9. *In vivo embolization study*

To examine occlusive ability of SPIO-chitosan MS, the embolized kidney was enucleated and stained by Prussian blue (Song et al., 2005). Histological examination revealed that the renal arteries were successfully obstructed by SPIO-chitosan MS, with SPIO nanoparticles identified by dark blue staining.

Both embolized and unembolized kidneys were bisected vertically to locate the SPIO-chitosan MS. The right kidney contained SPIO-chitosan MS located in the main and segmental renal arteries, while the left kidney was devoid of any embolic materials. The embolized kidney was paler than the unembolized kidney, due probably to ischemia caused by the blocked renal arteries, which is additional evidence that the embolization was successful.

4. Conclusions

In this study, MR traceable and deformable SPIO-chitosan MS were successfully prepared by ionotropic gelation and PEG leaching. The SPIO-chitosan MS were spherical and highly deformable and could efficiently be delivered through a microcatheter used for anti-cancer embolotherapy. The location and retention of embolized SPIO-chitosan MS in rabbit renal arteries were monitored by MRI for 18 weeks. Therefore deformable SPIO-chitosan MS can be possibly used as a multifunctional embolic material for anti-cancer embolotherapy. Their MR traceability would be advantageous for following the embolization outcome.

Acknowledgement

This work was supported by Mid-career Researcher Program through NRF grant funded by the MEST (No. 2010-0027798).

References

Agnihotri, S. A., Mallikarjuna, N. N., & Aminabhavi, T. M. (2004). Recent advances on chitosan-based micro- and nanoparticles in drug delivery. *Journal of Controlled Release*, *100*, 5–28.

Beaujeux, R., Laurent, A., Wassef, M., Casasco, A., Gobin, Y. P., Aymard, A., et al. (1996). Trisacryl gelatin microspheres for therapeutic embolization. II: Preliminary clinical evaluation in tumors and arteriovenous malformations. *American Journal of Neuroradiology*, *17*, 541–548.

Bendszus, M., Klein, R., Burger, R., Warmuth-Metz, M., Hofmann, E., & Solymosi, L. (2000). Efficacy of trisacryl gelatin microspheres versus polyvinyl alcohol particles in the preoperative embolization of meningiomas. *American Journal of Neuroradiology*, *21*, 255–261.

Chung, J., Yamada, M., & Yang, P. C. (2009). Magnetic resonance imaging of human embryonic stem cells. In *Current protocols in stem cell biology*.

Derdeyn, C. P., Graves, V. B., Salamat, M. S., & Rappe, A. (1997). Collagen-coated acrylic microspheres for embolotherapy: In vivo and in vitro characteristics. *American Journal of Neuroradiology*, *18*, 647–653.

Escobedo, E. M., Hunter, J. C., Zink-Brody, G. C., Wilson, A. J., Harrison, S. D., & Fisher, D. J. (1996). Usefulness of turbo spin-echo MR imaging in the evaluation of meniscal tears: Comparison with a conventional spin-echo sequence. *American Journal of Roentgenology*, *167*, 1223–1227.

Fischer, T. H., Thatte, H. S., Nichols, T. C., Bender-Neal, D. E., Bellinger, D. A., & Vournakis, J. N. (2005). Synergistic platelet integrin signaling and factor XII activation in poly-N-acetyl glucosamine fiber-mediated hemostasis. *Biomaterials*, *26*, 5433–5443.

Flandroy, P., Grandfils, C., Collignon, J. A., Thibaut, N., Nihant, S., Barbette, R. J., et al. (1990). (D,L) Polylactide microspheres as embolic agent. *Interventional Neuroradiology*, *32*, 311–315.

Grandfils, C., Flandroy, P., & Jerome, R. (1996). Control of the biodegradation rate of poly (DL-lactide) microparticles intended as chemoembolization materials. *Journal of Controlled Release*, *38*, 109–122.

Hamoudeh, M., Faraj, A. A., Canet-Soulas, E., Bessueille, F., Leonard, D., & Fessi, H. (2007). Elaboration of PLLA-based superparamagnetic nanoparticles: Characterization, magnetic behaviour study and in vitro relaxivity evaluation. *International Journal of Pharmaceutics*, *338*, 248–257.

Hultmark, D. (1996). Insect lysozymes. In P. Jolles (Ed.), *Lysozymes: Model enzymes in biochemistry and biology* (pp. 87–102). Switzerland: Birkhäuser Verlag.

Kang, M. J., Park, J. M., Choi, W. S., Lee, J., Kwak, B. K., & Lee, J. (2010). Highly spherical and deformable chitosan microspheres for arterial embolization. *Chemical and Pharmaceutical Bulletin*, *58*, 288–292.

Kassab, A. C., Piskin, E., Bilgic, S., Denkbas, E. B., & Xu, K. (1999). Embolization with polyhydroxybutyrate (PHB) microspheres: In vivo studies. *Journal of Bioactive and Compatible Polymers*, *14*, 291–303.

Laurent, A. (2007). Microspheres and nonspherical particles for embolization. *Techniques in Vascular and Interventional Radiology*, *10*, 248–256.

Llovet, J. M., Real, M. I., Montaña, X., Planas, R., Coll, S., Aponte, J., et al. (2002). Arterial embolisation or chemoembolisation versus symptomatic treatment in patients with unresectable hepatocellular carcinoma: A randomised controlled trial. *Lancet*, *359*, 1734–1739.

Moon, W. K. (2004). Molecular MR imaging. *Journal of the Korean Medical Association*, *47*, 133–138.

Muzzarelli, R. A. A. (1993). Biochemical significance of exogenous chitins and chitosans in animals and patients. *Carbohydrate Polymers*, *20*, 7–16.

Muzzarelli, R. A. A. (2009a). Chitins and chitosans for the repair of wounded skin, nerve, cartilage and bone. *Carbohydrate Polymers*, *76*, 167–182.

Muzzarelli, R. A. A. (2009b). Genipin-crosslinked chitosan hydrogels as biomedical and pharmaceutical aids. *Carbohydrate Polymers*, *77*, 1–9.

Muzzarelli, R. A. A. (2010). Chitins and chitosans as immunoadjuvants and nonallergenic drug carriers. *Marine Drugs*, *8*, 292–312.

Pepper, K. W., Reichenberg, D., & Hale, D. K. (1952). Properties of ion-exchange resins in relation to their structure. Part IV. Swelling and shrinkage of sulphonated polystyrenes of different cross-linking. *Journal of the Chemical Society*, 3129–3136.

Qiao, R., Yang, C., & Gao, M. (2009). Superparamagnetic iron oxide nanoparticles: From preparations to in vivo MRI applications. *Journal of Materials Chemistry*, *19*, 6274–6293.

Ren, D., Yi, H., Wang, W., & Ma, X. (2005). The enzymatic degradation and swelling properties of chitosan matrices with different degrees of N-acetylation. *Carbohydrate Research*, *340*, 2403–2410.

Rice, H. E., Hsu, E. W., Sheng, H., Evenson, D. A., Freemerman, A. J., Safford, K. M., et al. (2007). Superparamagnetic iron oxide labeling and transplantation of adipose-derived stem cells in middle cerebral artery occlusion-injured mice. *American Journal of Roentgenology*, *188*, 1101–1108.

Shomura, Y., Tanigawa, N., Shibutani, M., Wakimoto, S., Tsuji, K., Tokuda, T., et al. (2010). Water-soluble polyvinyl alcohol microspheres for temporary embolization: Development and in vivo characteristics in a pig kidney model. *Journal of Vascular and Interventional Radiology*, *22*, 212–219.

Song, Y. S., Lee, K. H., Park, Y. H., Kim, J. H., Choi, D. H., Jeon, J. S., et al. (2005). Histologic monitoring of the transplanted superparamagnetic iron oxide labelled human mesenchymal stem cells in the rat bladder. *Journal of the Korean Continence Society*, *9*, 102–107.

Thom, A. K., Sigurdson, E. R., Bitar, M., & Daly, J. M. (1989). Regional hepatic arterial infusion of degradable starch microspheres increases fluorodeoxyuridine (FUdR) tumor uptake. *Surgery*, *105*, 383–392.

Thorek, D. L., Chen, A. K., Czupryna, J., & Tsourkas, A. (2006). Superparamagnetic iron oxide nanoparticle probes for molecular imaging. *Annals of Biomedical Engineering*, *34*, 23–38.

Wang, Y. J. (2011). Superparamagnetic iron oxide based MRI contrast agents: Current status of clinical application. *Quantitative Imaging in Medicine and Surgery*, *1*, 35–40.

Widmaier, E. P., Raff, H., & Strang, K. T. (2006). *Vander's human physiology: The mechanisms of body function* (10th ed.). New York: McGraw-Hill., p. 383.

Wilson, M. W., Fidelman, N., Weber, O. M., Martin, A. J., Gordon, R. L., LaBerge, J. M., et al. (2003). Experimental renal artery embolization in a combined MR imaging/angiographic unit. *Journal of Vascular and Interventional Radiology*, *14*, 1169–1175.

Yuan, Y., Chesnutt, B. M., Utturkar, G., Haggard, W. O., Yang, Y., Ong, J. L., et al. (2007). The effect of cross-linking of chitosan microspheres with genipin on protein release. *Carbohydrate Polymers*, *68*, 561–567.